

## MULTI-TEMPORAL FLOOD MAPPING AND FARM FLOOD PREVENTION STRATEGIES IN AN AGRICULTURALLY DOMINATED WATERSHED OF ARGENTINA

### CARTOGRAFÍA MULTITEMPORAL Y ESTRATEGIAS PARA LA PREVENCIÓN DE INUNDACIONES EN UNA CUENCA CON PREDOMINIO AGRÍCOLA DE ARGENTINA

María Ximena Solana <sup>(1)</sup>, Asunción Romanelli <sup>(2)</sup> y Orlando Mauricio Quiroz Londoño <sup>(3)</sup>

Instituto de Investigaciones Marinas y Costeras, Consejo Nacional de Investigaciones Científicas y Técnicas, Facultad de Ciencias Exactas y Naturales; e Instituto de Geología de Costas y del Cuaternario, Universidad Nacional de Mar del Plata – Comisión de Investigaciones Científicas Provincia de Buenos Aires, Facultad de Ciencias Exactas y Naturales, Mar del Plata, Argentina.

<sup>(1)</sup> e-mail: ximenasolana@mdp.edu.ar. ORCID: <https://orcid.org/0000-0002-4575-6990>

<sup>(2)</sup> e-mail: aromanel@mdp.edu.ar. ORCID: <https://orcid.org/0000-0002-9003-396X>

<sup>(3)</sup> e-mail: qlondono@mdp.edu.ar. ORCID: <https://orcid.org/0000-0002-2817-9570>

#### ABSTRACT

This study presents a semi-automated approach for mapping the extent and frequency of floods in agriculturally dominated river watersheds, using the Quequén Grande River watershed as a case study. By the combination of normalized difference indices computed from Landsat imagery and the application of Otsu's thresholding method in Google Earth Engine (GEE) environment, two flood categories were defined: Open Flood Surfaces (OFS) and Flooded Vegetation (FV). The analysis of historical flood frequency allowed the proposal of flood prevention strategies to be implemented in each defined flood frequency class, which is essential for flood mitigation in agriculturally dominated river watersheds.

**Keywords:** Google Earth Engine, Landsat Imagery, Spectral Indices, Flood Mapping, Flood Prevention Strategies.

#### RESUMEN

En este estudio se propone un método semiautomático para la cartografía de la extensión y frecuencia de las inundaciones en una cuenca hidrográfica con predominio agrícola, seleccionándose la cuenca del Río Quequén Grande como caso de estudio. Mediante la combinación de índices diferenciales normalizados calculados a partir de imágenes Landsat y la aplicación del método de umbralización desarrollado por Otsu en el entorno de Google Earth Engine (GEE), se definieron dos categorías para las inundaciones: superficies de inundación abiertas (OFS) y vegetación inundada (FV). El análisis de la frecuencia histórica de las inundaciones permitió la propuesta de estrategias de prevención a las inundaciones dirigidas a ser implementadas en cada clase de frecuencia de inundación definida, siendo esencial para la mitigación de inundaciones en cuencas hidrográficas con predominio agrícola.

**Palabras clave:** Google Earth Engine, Imágenes Landsat, Índices Espectrales, Cartografía de inundaciones, Estrategias de Prevención a la Inundación.

## INTRODUCTION

Flooding is an extended natural hazard that affects the society of different parts of the world, and it is considered the most recurring and devastating problem from its impact on the economic and social conditions of human lives (Alderman et al., 2012; Wannous & Velasquez, 2017). The influence of human activity also enhances the severity and consequences of flooding events, which are generated by the arbitrary coincidence of different meteorological factors (Feloni et al., 2019). Global climatic change, land-use changes, and accelerated urbanization are intensifying flood events worldwide, independently of their topographic and meteorological context (Dash & Sar, 2020; Detrembleur et al., 2015; Du et al., 2015).

Predicting the potential flood inundation extent (*i.e.*, identifying areas susceptible to flooding) of heavy rainfall events is critical, particularly in developing countries where the effects of floods are severely felt (Dash & Sar, 2020). However, in most of these countries, the accessibility of flood inundation extent maps is scarce, and those existing are outdated and have a low spatio-temporal resolution (Mehmood et al., 2021). In Latin America and the Caribbean region (LAC) floods are the most common disaster, with 548 floods occurring since 2000 (UN-OCHA, 2020). Here, the intensification of flood consequences is expected due to several socio-economic and political factors such as inefficient public policies, infrastructural problems, poverty persistence, ineffective emergency response to flooding events, unregulated and exponential urbanization of floodplains, anthropogenic degradation of catchments, and the lack of flood data (Sandoval & Sarmiento, 2020; UN-OCHA, 2020).

Over the last decade, there has been a proliferation of Earth Observations (EO) data. The global open data access from operational satellites like the Landsat series, together with important advances in cloud computing, have made possible the cartography of inundation over increasingly larger scales (DeVries et al., 2020; Hawker et al., 2020; Mehmood et al., 2021), and at relatively high spatio-temporal resolution (Wulder & Coops, 2014). Particularly, the cloud-based platform Google Earth Engine (GEE) stands out. It was introduced by Google Inc. for planetary-scale geospatial analysis and provides free access to high-performance computing resources, allowing the processing of extensive geospatial datasets (Gorelick et al., 2017).

The development of this tool represents a great opportunity for effective flood response interventions and management plans, especially in under-resourced regions of the world with a lack of information (Hawker et al., 2020). In the case of flood inundation extent maps developed from satellite imagery, the creation of several algorithms has been produced by different institutions such as universities, space agencies, or companies directed to disaster recovery and response (DeVries et al., 2020; Hawker et al., 2020; Mehmood et al., 2021; Policelli et al., 2017). Specifically, for the Global South, most of the flood-related research including the use of GEE for flood extent identification is associated with South Asia (Kumar et al., 2022; Lal et al., 2020; Pandey et al., 2022; Vanama et al., 2020), with very few studies in LAC countries (Mora et al., 2021; Tellman et al., 2021).

In Argentina, extreme precipitation events causing floods and droughts lead to the country's natural hazard risk profile. Floods have been responsible for causing important economic losses since 1980, with an average of US \$ 1 billion annually (World Bank, 2021), and these losses could increase by 125% due to climate change. Recently, historical increases in the frequency of flooding linked to severe rainfall events highlighted the need for improved risk management strategies. This behavior can be partially attributed to higher average precipitation, land-use changes, and water table rising (Rozenberg et al., 2021). In the case of very flat and poorly drained landscapes, the rise in water tables causes floods linked to increased water storage, and after reaching high levels water losses occur as liquid water outflows, in addition to an increased evaporation rate (Fan et al., 2013; Kuppel et al., 2015).

The Argentine Pampa region (east-central of the country), is a subhumid aeolian plain that encompasses the most populated and productive sector of the country. Here, an alternation of non-flooded and flooding cycles occurs and describes the ephemeral nature of surface water coverage (Houspanossian et al., 2018), which makes this region highly relevant for implementing flood mapping techniques. During large episodic flood events, an important fraction of the sedimentary Pampean Plain is covered by water for months or even years, on account of low horizontal water transport caused by the low surface runoff and the slowness of groundwater flow (Aragón et al., 2011). The hydrological conditions of these very flat

regions must be considered carefully when land management strategies are implemented (Kuppel et al., 2015), especially because there is an expected intensification of farming at such arable lands since global food demand and trade are increasing (Paruelo et al., 2005).

This article presents a semi-automatic methodology for mapping the spatial extent and frequency of flooding in agriculturally dominated plain environments. Based on spectral indices computed at the GEE platform, our approach aims to generate historical flood frequency maps from past flood events that occurred between 2000 and 2020. Additionally, the proposed approach gives some advances in the detection and extraction not only of open flood surfaces but also of flooded areas underneath vegetation (*i.e.*, flooded vegetation), which is of particular importance for flood monitoring and assessment. By conducting a comprehensive multi-temporal assessment of floods in an agriculturally dominated watershed, we sought to achieve the following results: i) identify areas with a history of frequent flooding, providing critical information to authorities and farmers regarding the flood-prone regions within the area, and ii) enable action guidelines for private landowners and agricultural producers to reduce the extent and impact of flood-related damage.

## STUDY AREA

To analyze the usefulness of the generated algorithm, a representative plain river watershed of the Pampa Region is proposed as a case study. The Quequén Grande River Watershed (QGRW) is an extensive river catchment located in an agricultural-livestock area of great economic importance for the country, with several small and medium-sized cities. Towards the southwest of the Tandilia Range System (TS), the origin of the Quequén Grande River (QGR) is marked by an undulating plain with a dominant northwest-southeast slope called “Pampa de Juárez”, and flows to the southeast across the Pampean Plain, reaching the Atlantic Ocean near Necochea city (Campo de Ferreras & Piccolo, 1999). Tributaries of this main water course are small streams developed almost exclusively from its right bank (Marini & Piccolo, 2005). From the hydrological point of view, this catchment belongs to a temperate climate zone where the mean annual precipitation in the basin is about 800 mm. However, the area is characterized by climatic

oscillations and instabilities, with a history of both floods and drought periods.

The QGRW comprises six geomorphological units, *i.e.*, ranges, perirange aeolian hills, relic hills, alluvial plain, poor drainage alluvial plain, and hills with shallow lakes (Teruggi et al., 2005) (Figure 1). Here, agriculture predominates over livestock farming, especially through the cultivation of wheat, natural pastures, and winter fodder cereals (Campo de Ferreras & Piccolo, 1999). The QGRW covers a surface of about 11000 km<sup>2</sup> and most of it consists of an essentially flat plain with a topographic average gradient of 0.03 (Teruggi et al., 2005). In the north part of the catchment area, a small sector is taken up by low-relief ranges (maximum elevation = 510 m a.s.l.) corresponding to the TS.

Hydrogeologically, the loess sediments of the Pampean Plain constitute an aquifer of great importance for the country, ranging between 70 - 100 m in thickness. This hydrogeological sequence represents an unconfined, shallow, and multi-layer aquifer, with permeability changes caused by subtle grain size and clay content variations (Martínez & Bocanegra, 2002). Groundwater recharge of this area is attributed mainly to precipitation, with groundwater discharge occurring towards the Atlantic Ocean, the surface drainage network (*i.e.*, rivers and streams), and the shallow lakes located at the southwestern limit of the QGRW. Here, a hydraulic barrier to the Pampean Aquifer has been proposed in-depth acting as a regional discharge area (Solana et al., 2021a). Rivers and streams are primarily effluents along their course, with south and/or southeast direction usually aligned to the groundwater flow path. For the QGR, a base-flow estimation of 70-90% was obtained (Martínez et al., 2010).

## MATERIALS AND METHODS

The proposed flood mapping code was developed in the GEE JavaScript API. This algorithm generates a stack of spatially overlapped pixels classified as water/non-water corresponding to the rainiest years between 2000 and 2020. Surface water changes were analyzed at the GEE platform by processing freely-available Surface Reflectance (SR) cloud products of Landsat 5 TM, Landsat 7 ETM+, and Landsat 8 OLI/TIRS imagery. To exclude permanent water bodies from flooded areas, the driest year of this period was also analyzed, and permanent water

bodies (*i.e.*, rivers, streams, and shallow lakes) were masked. Water detection was achieved by the combination of two normalized difference indices: the Modified Normalized Difference Water Index (MNDWI; Xu, 2006) and the Normalized Difference Vegetation Index (NDVI; Tucker, 1979). Then, Above-Ground Water Presence Frequency (AWPF) maps were obtained following Borro et al. (2014). The proposed code consists of five steps: (1) free

data selection from cloud servers, (2) pre-processing of Landsat imagery, (3) normalized difference indices computation and dynamic segmentation, (4) water detection, (5) multi-temporal flood analysis, and (6) mapping of flooding frequency. The methodological framework is shown in Figure 2. The generated GEE JavaScript codes for multi-temporal flood analysis and mapping of flooding frequency are provided in *Data Availability*.

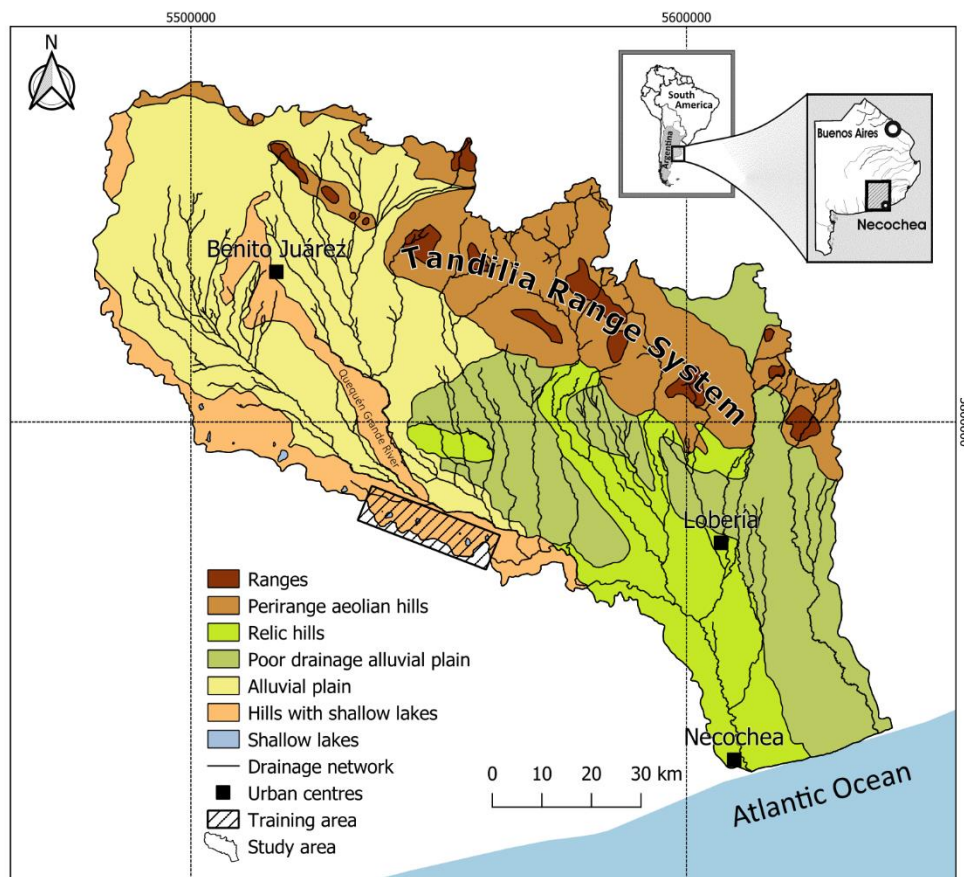


Figure 1: Location and geomorphologic units of the study area.

### Data selection

To evaluate rainfall trends in the study area, precipitation data from the last 60 years were reviewed. Time series of daily rainfall data (mm/day) within the influence area of the QGRW were extracted from national and local weather stations (National Institute of Agricultural Technology-INTA, Meteorological National Service-SMN, National University of Mar del Plata-UNMDP). All rainfall time series from the period were analyzed and processed to obtain both a

monthly mean value and an annual total value per year. Finally, those years between 2000 and 2020 with annual rainfall values reaching one standard deviation above the mean precipitation value of the last 60 years were selected as target years for flooding mapping. Additionally, the driest year of this period (*i.e.*, 2009) was selected for the generation of an exclusion mask of permanent water bodies from flooded areas. Regarding remote sensing data, SR cloud products from Landsat 5 TM, Landsat 7 ETM+, and Landsat 8 OLI/TIRS were selected from the Earth Engine Data Catalog.

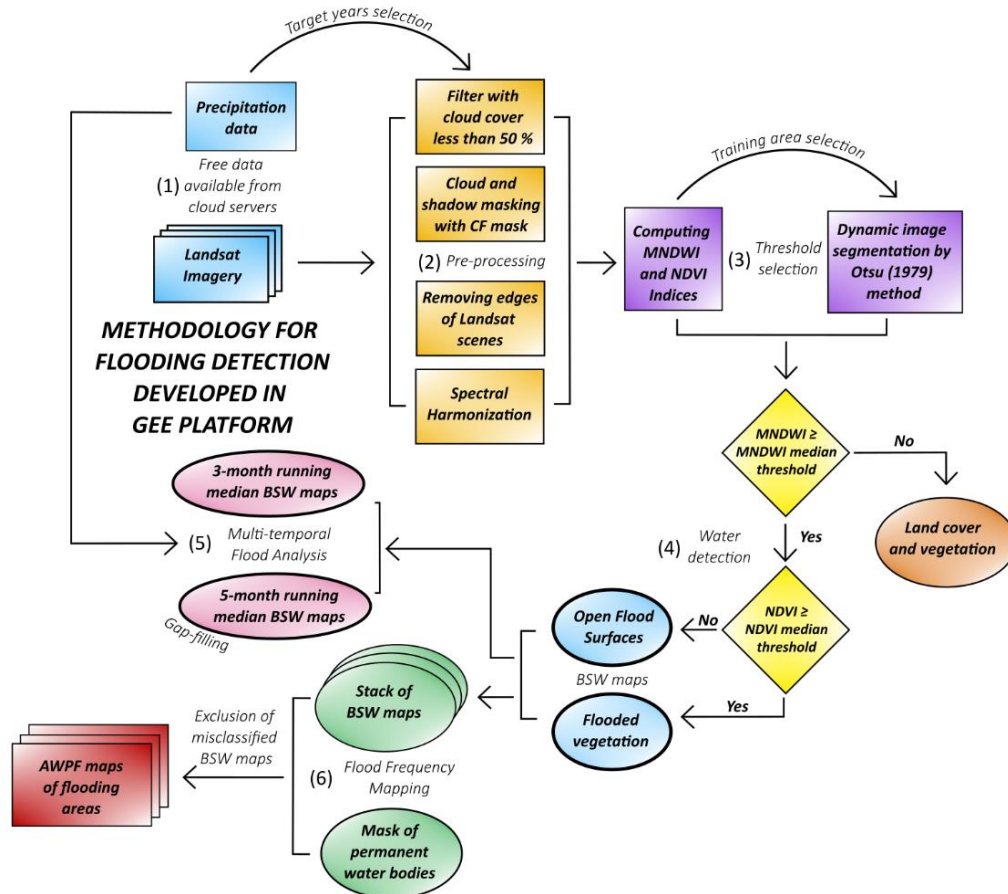


Figure 2: Schematic workflow of the flood extension and frequency mapping, developed in the GEE environment. Each of the six steps is indicated by parentheses.

### Pre-processing of Landsat imagery

Landsat satellite imagery was initially filtered by a cloud cover of less than 50%. Then, shadow and cloud masking were performed using the pixel quality assurance band (qa) with the C Function of Mask (CFMask) algorithm. The CFMask series of algorithms are recommended for the operational detection of clouds and cloud shadows at the Landsat series, as they are based on a previous understanding of such physical phenomena and can be implemented with no geographical restrictions (Foga et al., 2017). Additionally, scene edges of all datasets were removed by clipping a buffer of 500 m inward as a way to exclude no-data pixels such as abnormalities along Landsat 5 scene edges (Robinson et al., 2017). Spectral characteristics of Landsat datasets were also harmonized by a linear transformation of OLI to TM /ETM+ spectral space

following Roy et al. (2016), in order to improve temporal continuity between sensors.

### Normalized difference indices computation and dynamic segmentation

The two normalized difference indices selected for water detection were computed by the following equations:

$$NDVI = \frac{NIR - R}{NIR + R} \quad (1)$$

Where *NIR*: near-infrared band and *R*: red band.

$$MNDWI = \frac{G - SWIR}{G + SWIR} \quad (2)$$

Where *G*: green band and *SWIR*: short-wave infrared band.

The segmentation threshold of each index was estimated by the Otsu (1979) method for a training area where differences between land, vegetation, and water can be easily distinguished. This dynamic method was selected since it automatically selects a threshold from two mixed distributions through the density histogram, which eliminates the bias caused by arbitrary thresholding methods. For the selected time-lapse collection, median threshold values were determined because they represent points where the sums of the distances from the representative points of the sample are a minimum (Haldane, 1948). Once obtained, NDVI and MNDWI median thresholds were applied to the entire study area.

### Water detection

By the calculation [equations (1) and (2)] and combination of the selected indices, more accurately flooded surface detection was achieved. Firstly, pixels with MNDWI values above the median threshold were identified as water. Then, an additional filter with NDVI values was applied to the pixel selection of MNDWI for each Landsat scene, in order to discern between open water surfaces and flooded vegetation. The proposed sub-selection was based on the NDVI response to inundation since areas adapted to flood pulses are highly responsive, showing increases and peaks in NDVI values (Powell et al., 2014). Finally, two categories were defined as follows:

- a. Open Flood Surfaces (OFS): represented by pixels with MNDWI values above the median threshold and NDVI values below the median threshold. This category corresponds mainly to wetlands, ponds, rivers, streams, and open water surfaces.
- b. Flooded vegetation (FV): represented by pixels with MNDWI and NDVI values above median thresholds. In the scope of this paper, the term FV describes the temporary or permanent occurrence of a water surface beneath vegetated areas (Tsyganskaya et al., 2018). It corresponds to wetland vegetated areas, floodplains, and surrounding stream areas covered by water during inundation events.

### Flooding evolution analysis

After OFS and FV detection of the selected Landsat scenes, Binary Surface Water (BSW) maps

corresponding to each category were obtained. Multi-temporal flood analysis was performed quarterly by running time-lapse collections of Landsat images and computing median BSW maps, since almost all the pixels of the QGRW surface were covered successfully after cloud masking (QGRW surface covered accuracy of about 99%). The selection of the quarterly multi-temporal flood analysis was based on the accuracy of the proposed algorithm at different time-lapse windows (*i.e.*, monthly, bimonthly, and quarterly). To achieve better results, a cut-off tolerance threshold value of 1 was set, *i.e.*, the total number of flooding maps obtained for the QGRW with a surface-covered accuracy lower than 80%, which was obtained quarterly. Additionally, pixels with no data values were filled by median BSW values of an additional 5-month running time-lapse collection of Landsat images.

### Mapping of flooding frequency

Annual flooding frequency was analyzed in each pixel of the QGRW using the entire Landsat collection of the target years. The applied methodology was based on the procedure defined by Borro et al. (2014), which is defined by the following equation:

$$AWPF_{sj} = \frac{\sum_{i=1}^{N_s} BSW_{ij}}{N_s} \quad (3)$$

Where  $AWPF_{sj}$  represents the above ground water presence frequency value of the pixel  $j$  for the set  $s$  and corresponds to the ratio of images  $i$  with BSW equal to 1 in the pixel  $j$  ( $BSW_{ij}$ ) of the total number of images in the analyzed set ( $N_s$ ). As a result, AWPF maps describing the water permanence degree in each pixel were obtained, ranging from 0 (pixels equal to 0 in all BSW maps) to 1 (pixels equal to 1 in all BSW maps). This methodology was successfully applied by Solana et al. (2021b) for the water frequency classification of shallow lakes located in the southwestern limit of the QGRW.

To exclude permanent water bodies from flood mapping, an exclusion mask was generated by the flooding frequency analysis of the driest year of this period (*i.e.*, 2009). Only the pixels labeled as permanent water (*i.e.*, AWPF pixels equal to 1 obtained for the driest year) have been included in the reference water mask. In every pixel of the watershed, each flood category (*i.e.*, Open Flood Surfaces -OFS- and Flooded Vegetation -FV-) was classified according to the relative frequency of occurrence of

the flooded area. For this purpose, five flood frequency classes were defined: *Very Low* (AWPF < 20%), *Low* (20% ≤ AWPF < 40%), *Moderate* (40% ≤ AWPF < 60%), *High* (60% ≤ AWPF < 80%), and *Very High* (AWPF ≥ 80%), taking as a reference the total number of handled images. Here, the exclusion of some BSW maps from the GEE code was required, since some Landsat scenes were affected by satellite malfunctions, and cloud shadows are not always successfully removed by the CFMask algorithm. However, excluded Landsat scenes from data processing only represented a small portion (12%) of the evaluated dataset (619 images). Satellite data distortion problems such as data loss are widely described on USGS official website (United State Geological Survey [USGS], access date 08/05/2023).

Finally, historical flood frequency maps were generated by combining all annual datasets of OFS and FV categories, and classified according to the relative flood frequency previously defined following Borro et al. (2014). Subsequently, a set of flood prevention strategies was proposed for each specific frequency class. These recommended measures are intended to assist farmers and landowners in reducing flood-related damages on farmlands and agricultural landscapes,

safeguarding agricultural productivity and minimizing potential losses.

## RESULTS

### Rainfall analysis

Annual and monthly average values of precipitation data are shown in Figure 3. In the case of total annual precipitation, a mean value of 858 mm was obtained for the last 60 years, showing a clear increasing tendency. In the case of monthly rainfall averages, the mean value reached 74 mm, but the increasing tendency was less clear. The greatest annual rainfall averages with values reaching one standard deviation (*i.e.*, 161.4 mm) above mean precipitation were obtained for 5 years. For those years, variations between monthly average values and mean precipitation of each month registered during the last 60 years showed, in most cases, average rainfall values above mean monthly precipitation (Figure 3). This behavior was especially noticed during the second half of the year. Moreover, four of the greatest annual rainfall years showed similar rainfall averages in August, with a subsequent decrease in September and a substantial increase in October and November.

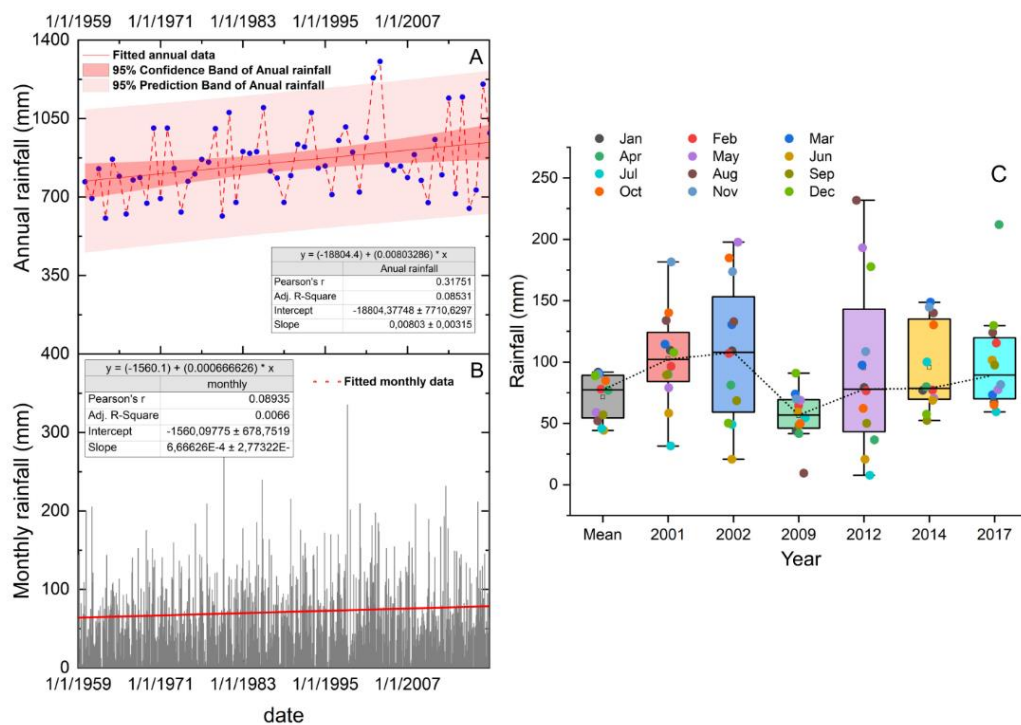


Figure 3: A) Annual and B) Monthly rainfall values between 1959 and 2020 for the study area. C) Box plots of monthly rainfall amounts in the target years of the study and mean rainfall values for the period 1959-2020.

### Changes in accumulated rainfall and flooded extension

Comparisons between quarterly accumulated precipitation (mm), open flood surfaces (km<sup>2</sup>), and flooded vegetation (km<sup>2</sup>) of the target years are shown in Figure 4. Results indicated water and flooded vegetation increase during the cold months of the winter (JJA, JAS), which can be attributed to the descent of evapotranspiration. In the case of precipitation, an increase is observed during the summer season, being the general tendency for the study area. Furthermore, results obtained for the driest year of the selected time-lapse window (2009) can be attributed to the permanent water bodies of

the QGRW, since flooded vegetation areas were almost absent.

The extreme values of obtained Otsu's median thresholds, the number of Landsat images used, and the percentages of QGRW surface covered accuracy obtained at the multi-temporal flood analysis, are shown in Table 1. In the case of the 3-month running time-lapse analysis, accuracy was defined as the percentage of the total study area covered by the handled quarterly Landsat collection, which was improved by the proposed gap-filling method of an additional 5-month running time-lapse collection, reaching values closer to 100% of accuracy.

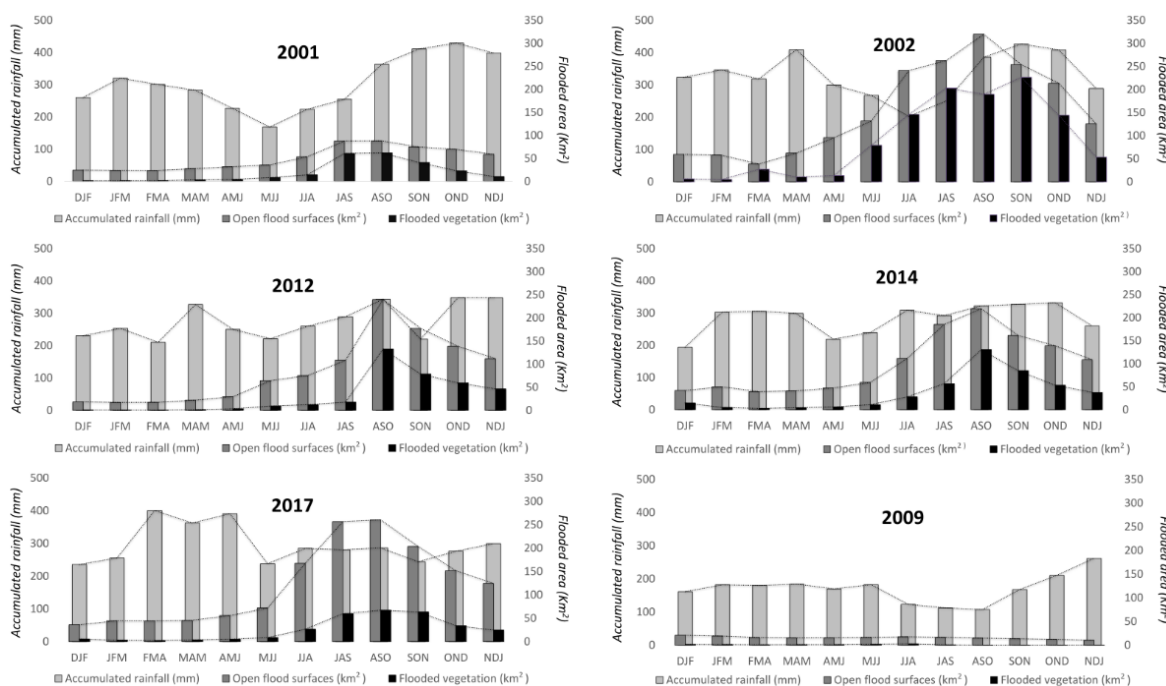


Figure 4: Accumulated rainfall (mm), open flood surfaces extension (km<sup>2</sup>), and flooded vegetation (km<sup>2</sup>) of the target years, expressed quarterly.

Table 1. Extreme values of Otsu's median thresholds, number of Landsat images, and percentages of accuracy obtained at the multi-temporal flood analysis for each year.

Year	Otsu's MNDWI		Otsu's NDVI		Quarterly Landsat		3-month		Final	
	median thresholds		median thresholds		Collections (#)		accuracy (%)		accuracy (%)	
	Min	Max	Min	Max	Min	Max	Min	Max	Min	Max
2001	-0.0393	0.0385	0.4139	0.4609	17	36	99.54	100.00	99.99	100.00
2002	-0.1175	0.0077	0.2733	0.5078	13	32	54.44	100.00	88.41	100.00
2009	-0.1020	-0.0073	0.3671	0.4766	8	39	51.24	100.00	99.34	100.00
2012	-0.1487	-0.0375	0.3356	0.5391	11	23	97.63	100.00	99.58	100.00
2014	-0.2577	-0.1794	0.3633	0.5391	21	45	99.98	100.00	99.99	100.00
2017	-0.2384	-0.1990	0.3633	0.5352	26	36	99.98	100.00	99.99	100.00

**Annual flood frequency maps**

AWPF maps of the selected years corresponding to OFS and FV frequency are shown in Figure 5. In the case of 2002, obtained results showed the maximum flooding extension (1398.84 km<sup>2</sup>), being specially noticed in the flooded vegetation category (802.21 km<sup>2</sup>). This was also observed in Figure 4, where the FV of 2002 showed an important increase, especially during the autumn season. Moreover, FV areas were located primarily at the floodplains of rivers and streams placed at the alluvial plain, which suggests an overflow caused by soil water surplus

generated in 2001, when soil water storage capacity reached its limit of absorption and storage capacity (Quiroz Londoño et al., 2013; Scarpati & Capriolo, 2013). In the case of 2014, the OFS total extension (653.74 km<sup>2</sup>) was greater than the FV category (297.22 km<sup>2</sup>). In regards to the driest year of the selected time-lapse window (2009), water corresponded primarily to permanent shallow lakes (8.51 km<sup>2</sup>), and FV (13.48 km<sup>2</sup>) was linked to the OFS (58.18 km<sup>2</sup>) or some isolated croplands with a very low flooding frequency. Flooding extension areas of each category of annual AWPF maps are shown in Table 2.

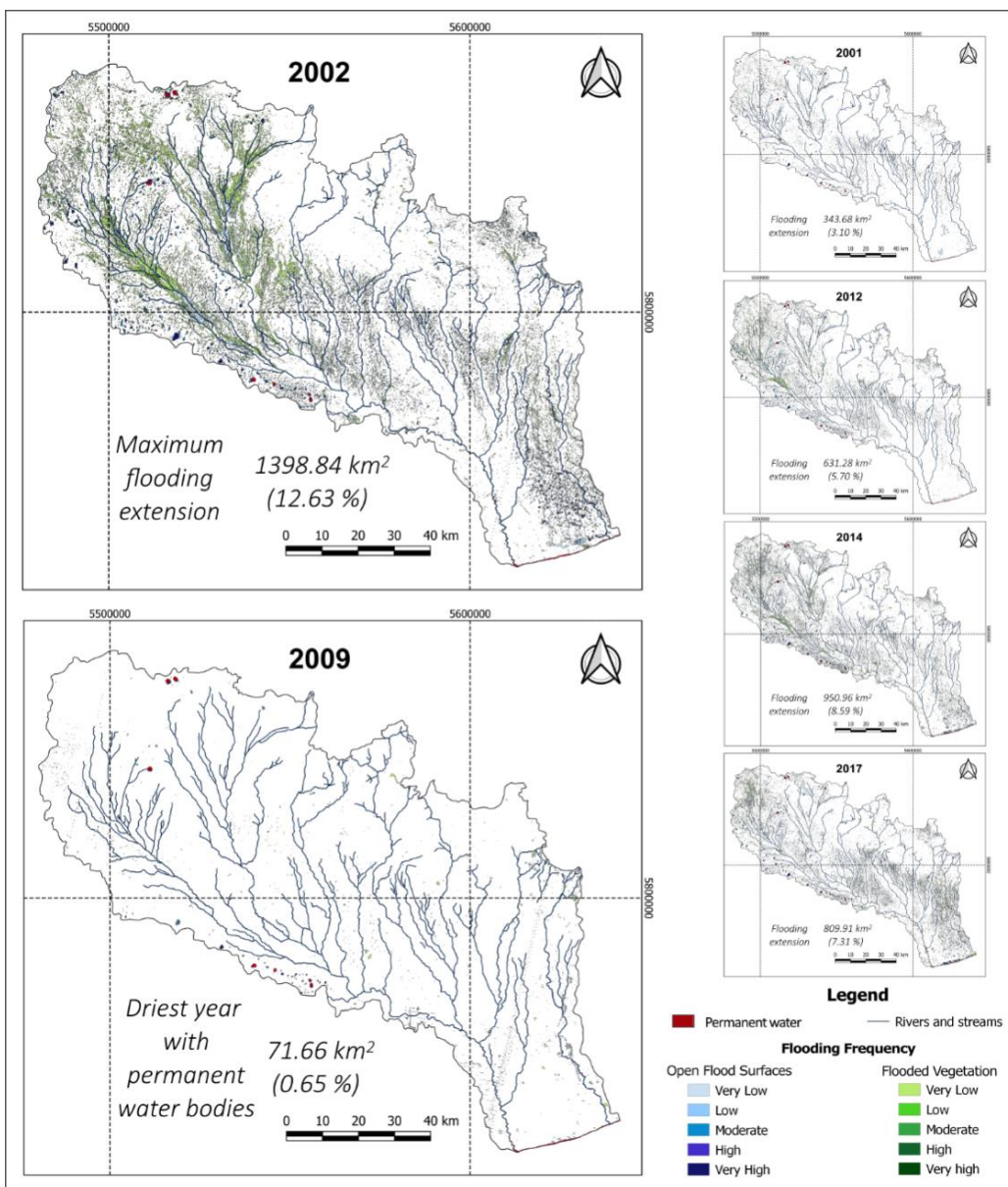


Figure 5: Flooding frequency in the QGRW obtained from Landsat imagery at the GEE platform for the selected years.

**Table 2. Flooding extension of the OFS and FV categories obtained for the QGRW from AWPf maps shown in Figure 5.**

Year	Flooding Surfaces(km <sup>2</sup> )										Handled Landsat		Otsu's median	
	Open Flood Surfaces					Flooded Vegetation					Images (#)		thresholds	
	Very Low	Low	Moderate	High	Very High	Very Low	Low	Moderate	High	Very High	Used	Excluded	MNDWI	NDVI
2001	216.4	24.4	6.0	4.7	19.8	70.7	1.6	0.02	-	-	94	10	0.0071	0.4610
2002	439.5	71.4	38.0	16.5	31.2	732.7	62.7	5.1	0.92	0.70	75	6	-0.0708	0.2735
2009	39.7	3.5	1.6	2.1	11.2	13.3	0.1	-	0.02	-	83	31	-0.0714	0.4141
2012	217.3	82.5	46.5	10.1	16.7	238.4	19.0	0.8	0.04	-	62	5	-0.1327	0.4299
2014	492.2	88.5	31.5	11.7	29.8	293.8	3.1	0.3	0.02	-	119	10	-0.2110	0.4414
2017	359.2	84.4	52.0	32.4	17.1	256.8	7.2	0.7	0.1	0.03	106	18	-0.2304	0.4336

### Final flood frequency maps

AWPF final maps corresponding to OFS and FV categories are shown in Figure 6. For the OFS category, all flooding frequencies were identified in the final map, reaching a total area of 1116.18 km<sup>2</sup>

and corresponding mainly to wetlands and ponds. In the case of FV, flooded areas were identified with *Very Low*, *Low* and *Moderate* frequencies of flooding, reaching a total area of 1520.29 km<sup>2</sup> located mainly at the floodplains of rivers and streams.

### Flooding Frequency

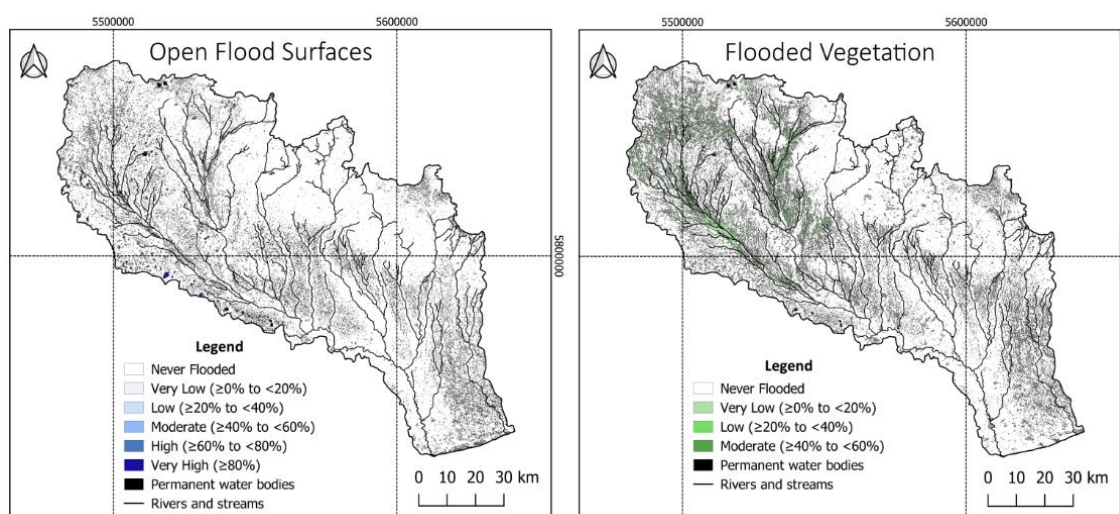


**Figure 6: Final flood frequency maps obtained for the study area with the selected time-lapse collection.**

The combination of historical OFS and FV binary maps, classified by the relative flood frequency classes, is shown in Figure 7. According to the geomorphologic units of the QGRW, the alluvial plain showed the maximum flooding extension (941.41 km<sup>2</sup>), reaching the 27.22% of the floodplains of rivers and streams (Table 3). Here, the FV category generates the greatest flooding impact (71%), which is related to overflows of the surrounding vegetated areas, corresponding mainly to the *Very Low* frequency class. In the poor drainage

alluvial plain, maximum flooding extension reaches 440.3 km<sup>2</sup>, which represents the 17.40% of this geomorphologic unit, and it is more represented by the OFS category (55%), corresponding to subcircular ponds with sizes ranging from 0.014 to 1.10 km<sup>2</sup> and minor ephemeral streams, as observed by Teruggi et al. (2005). Similar results were obtained in the hills with shallow lakes, with a maximum flooding extension of 195.49 km<sup>2</sup> (17.14% of the hills extension) and represented mainly by the OFS category (60%). Particularly in this area, the

*Very High* frequency class is better represented (9.88 km<sup>2</sup>), since temporary water bodies related to the subsurface water flow emerge. In the case of the relic hills and perirange aeolian hillocks, maximum flooding extension was lower (92.11 km<sup>2</sup> and 93.79

km<sup>2</sup>), covering the 5.91% and the 4.45% of the total extension of the mentioned geomorphologic units, respectively. Finally, as expected, flooding in the ranges was almost negligible (7.98 km<sup>2</sup>, representing 2.88% of the range system).

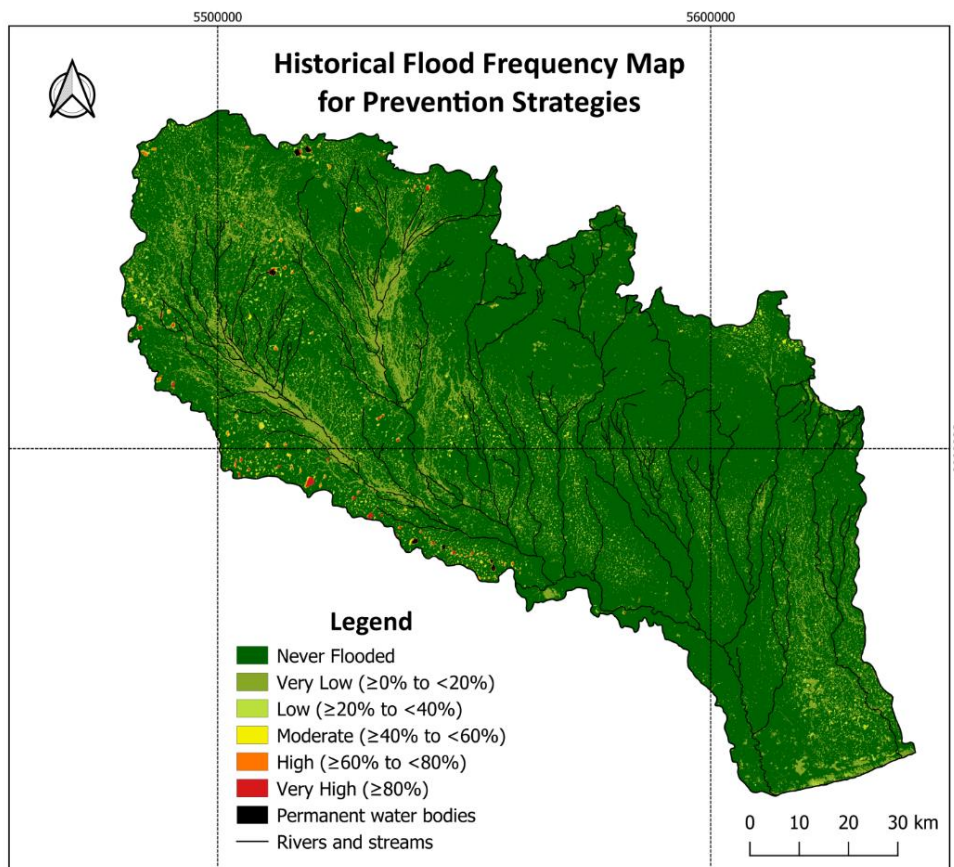


Figure 7: Historical Flood Frequency Map conducted to determine flood prevention strategies in the region.

Table 3. Flood extension of the historical flood frequency obtained for the geomorphologic units of the QGRW.

Geomorphologic unit	Area (km <sup>2</sup> )							TOTAL (Flooded)	Area (%) Flooded	Flooding representation	
	Total area	Not flooded	Very Low	Low	Moderate	High	Very High			FV (%)	OFS (%)
<i>Ranges</i>	277	269.1	7.89	0.09	-	-	-	7.98	2.88	61	39
<i>Perirange aeolian hills</i>	2110	2016.19	86.94	3.8	2.09	0.85	0.11	93.79	4.45	52	48
<i>Relic hills</i>	1557	1465.44	82.36	6.77	1.8	0.68	0.5	92.11	5.91	39	61
<i>Hills with shallow lakes</i>	1141	945.31	129.18	33.86	14.17	8.4	9.88	195.49	17.14	40	60
<i>Alluvial plain</i>	3459	2517.41	879.65	45.16	9.23	4.55	2.82	941.41	27.22	71	29
<i>Poor drainage alluvial plain</i>	2531	2090.6	370.06	53.97	13.97	1.87	0.43	440.3	17.4	45	55
<b>TOTAL</b>	<b>11075</b>	<b>9304.05</b>	<b>1556.08</b>	<b>143.65</b>	<b>41.26</b>	<b>16.35</b>	<b>13.74</b>	<b>1771.08</b>	<b>15.99</b>	<b>51</b>	<b>49</b>

## Flood prevention strategies

Farm flood prevention strategies can vary depending on specific circumstances and location. However, there are certain agricultural best management practices and measures that each single landowner and agricultural producer can implement for farm flood prevention (Antolini et

al., 2020; European Commission - Directorate-General for Environment, 2021; Warner et al., 2017). Based on the results of the historical flood frequency mapping (Figures 6 and 7), several flood prevention measures were proposed for implementation in each flood frequency class (Table 4), encompassing both structural and non-structural approaches.

**Table 4. Recommended strategies for farm flood prevention based on flood frequency classes.**

Flood prevention strategies	Flood frequency classes		
	<i>Low-Very low flood frequency</i>	<i>Moderate flood frequency</i>	<i>High-Very high flood frequency</i>
1. Land Use Planning	**	***	****
2. Drainage Management	*	***	****
3. Conservation practices		**	****
4. Buffer Zones		***	****
5. Erosion Control	*	***	****
6. Floodplain Management		***	****
7. Water Storage and Detention		**	****
8. Soil Management	**	***	****
9. Communication and Education	*	**	****
10. Monitoring	**	***	****
11. Flood insurance	*	***	****

*Very high (\*\*\*\*), high (\*\*\*), moderate (\*\*), low (\*), or insignificant (empty cell) indicate the recommended actions for flood prevention regarding each flood frequency class*

1. Land use planning: Proper land use planning is essential to minimize the risk of flooding on farms. Avoiding construction or farming activities in flood-prone areas can help prevent flood damage. Identify areas at higher elevations or well-drained soils for critical infrastructure and sensitive operations.

2. Drainage management: Implementing effective drainage systems is crucial for both high and low flood frequency scenarios. Maintain and regularly inspect existing drainage ditches, channels, and culverts to ensure they are clear of debris and functioning properly. Consider installing additional drainage infrastructure if necessary.

3. Conservation practices: Implement conservation practices that promote soil health and water infiltration. Practices like contour plowing, strip cropping, cover cropping and planting trees can help reduce surface runoff and improve soil structure, decreasing the risk of flooding.

4. Buffer zone and wetland restoration: Establish buffer zones or riparian buffers along water bodies, such as rivers or streams, adjacent to the farm. These natural vegetated areas can help absorb excess water during floods, reduce erosion, and filter out sediment and pollutants.

5. Erosion control: Implement erosion control measures to prevent soil erosion, which can worsen flooding. Methods such as terracing, grassed waterways, and retaining walls can help minimize erosion and keep soil in place.

6. Floodplain management: If your farm is located in a floodplain, it's important to understand the flood risks and develop appropriate floodplain management strategies. This may include strategies like floodplain zoning, flood forecasting, early warning systems, and emergency response planning.

7. Water storage and detention: Constructing on-farm water storage and detention structures, such as ponds or reservoirs, can help capture excess water during high flood events. These structures can also be used for irrigation during dry periods.

8. Soil management: Maintaining healthy soils through practices like organic matter management and appropriate crop rotation can improve soil structure and water-holding capacity, reducing the impact of flooding.

9. Communication and education: Promote awareness and education among farm owners, workers, and neighboring communities about flood risks and appropriate flood prevention measures.

Encourage collaboration with local authorities, extension services, and other stakeholders involved in water management.

10. Monitoring networks (data and information): Effective monitoring is widely acknowledged as a critical component of prediction and prevention strategies. In particular, the establishment of stream/river gauges for continuous streamflow monitoring, systematic recording and analysis of precipitation patterns and regular monitoring of water table levels are of paramount importance. Additionally, the installation of on-farm weather stations can provide invaluable insights to farmers, enabling them to plan and prepare for extreme weather conditions and optimize their planting and harvesting schedules.

11. Flood insurance: Can help farmers prepare for and recover from such disasters.

## DISCUSSION

During the last years, the production of low-cost flood maps all around the globe has increased, since several satellite datasets were made available for free (Hawker et al., 2020; Mehmood et al., 2021). The analysis of long time series of multi-temporal satellite imagery, as applied in this study, proved to be useful information for generating flood maps. In this contribution, an evaluation tool to translate flood data into operational maps is provided, which allows visualizing the spatial dimension of potential floods and taking action to prevent and reduce their damage.

The proposed method has several strengths: firstly, cloud-cover and shadow limitations in the performance of normalized difference indices have been overcome by including image pre-processing procedures (e.g., C Function of Mask algorithm, collection filtering). Secondly, the temporal continuity of reflectance between Landsat TM, ETM+, and OLI/TIRS sensors was undertaken by spectral harmonization following Roy et al. (2016), which allowed the analysis of long-time series of multiple sensors properly. Thirdly, the proposed identification of flooded areas created by the combination of spectral indices (i.e., MNDWI and NDVI) provided more accurate information related to the associated flooding events. In this sense, the NDVI proved to be a powerful tool to differentiate between open water surfaces and flooded vegetation previously detected as water by MNDWI, as the

NDVI response during flood events is highly sensitive to inundation (Powell et al., 2014), and it is usually underestimated at flooding detection. Finally, the selection of a training area within the study area (i.e., watershed), where differences between water, land, and vegetation are exposed, was a key point to enhance the Otsu dynamic threshold selection of the utilized normalized difference indices for flood mapping of the QGRW.

Delineation of water and monitoring of water body changes have been successfully performed by the computation of Normalized Difference Water Indices (NDWI) worldwide (Jain & Sinha, 2005; McFeeters, 1996; Rogers & Kearney, 2004; Sethre et al., 2005; Xu, 2006, among others). Particularly, the MNDWI proposed by Xu (2006) is the best option for delineating surface water in Landsat imagery, since it improves the separation of built-up features and vegetation (Campos et al., 2012; Mohammadi et al., 2017) from water. However, the threshold between water and non-water features is not a constant value; instead, it is a dynamic value that changes according to the subpixel land-cover components. Thus, for a given water fraction, the thresholds can be determined more efficiently by examining the histogram of the MNDWI image (Ji et al., 2009). In this sense, Otsu's threshold selection method for gray-level histograms is appropriate since it is simple, nonparametric, unsupervised, and automatic (Otsu, 1979). For a better implementation of this method, a training area with clear differences between the targets of the study (i.e., water, non-water) might be selected, and obtained thresholds can then be applied to the entire study area.

In the case of NDVI, several studies use this index to detect water and flooding (Domenikiotis et al., 2003; Shrestha et al., 2017). Nonetheless, it remains a vegetation index that is strongly sensitive to the subpixel vegetation component, which makes it less suitable for delineating water unless the SWIR band is not available in the remote sensor (Ji et al., 2009). Concerning flood events, very low values of NDVI are expected when the soil/vegetation component is flooded. But this behavior is different in areas adapted to the flood pulse (Powell et al., 2014). In the proposed study area, the subpixel components of floodplains located at rivers and streams, in addition to wetland vegetated areas are highly responsive to NDVI during flooding pulses. Thus, a combination of MNDWI and NDVI can be used that assess not only the open water flooding but also the productivity response to flooding, according to the

vegetation response. This combination of indices has been already used by several authors for monitoring flooding areas (Azedou et al., 2022; Mehmood et al., 2021; Solana et al., 2021b, among others). However, most of these studies focused on the detection of open water surfaces and disregarded the FV class, which can lead to an underestimation of the extent of inundation. The present work gives some advances in the detection and extraction not only of open flood surfaces but also of flooded areas underneath vegetation, allowing the creation of much more realistic scenarios of flooding.

In the QGRW, differences between the spatial distribution and frequency of potential floods in both OFS and FV can be attributed to the watershed dynamics of this poorly drained landscape. Regarding OFS, the *Moderate* to *Very High* flood frequency categories were observed mainly in temporary water bodies. This was particularly evident in the hills with shallow lakes located at the southwestern limit of this plain river watershed, where Solana et al. (2021a) proposed a regional discharge area associated with the presence of a hydraulic barrier to the Pampean aquifer in-depth. Similar behavior was observed in the poorly drained alluvial plain, where the *Very Low* to *Moderate* frequency categories of both OFS and FV can be attributed to the groundwater rise. In this sense, it has been recently observed in the South American plains that initial deep groundwater levels do not recover because of the replacement of natural pastures and native vegetation by rainfed agriculture, which leads to flooding even under low rainfall scenarios (Houspanossian et al. 2023). Conversely, the *Very Low* flood frequency category of OFS also occurred in the main rivers, which may be related to important but isolated overflows. In the case of FV areas, the *Very Low* to *Moderate* categories were observed primarily in floodplains along rivers and streams, which can be related to the typical discharge behavior of these watercourses that flood along surrounding croplands.

Flood mapping in other basins with similar geographical, climatological, and geomorphological features could apply the method followed in this study by adapting the algorithm and adjusting the thresholds for detecting floods in comparable areas, for future implementation of flood prevention strategies. By engaging in good planning and making strategic investments, private landowners and agricultural producers can proactively prevent flooding and safeguard their land interests and

assets. While farmers cannot entirely prevent flooding, they can significantly reduce the potential damage and negative impacts on their agricultural operations by implementing these strategies and taking appropriate actions. It is crucial for farmers to assess their specific circumstances, local conditions, and flood risk profiles to determine the most appropriate combination of flood prevention measures for their farms. Additionally, staying updated with local regulations, guidelines, and best practices related to flood management is essential.

## CONCLUSIONS

This study contributed to the generation of flood inundation extent and frequency maps along rivers in plain watershed basins, which is of particular importance for flood monitoring and assessment of these environments. By using the advantages offered by the GEE platform, the historical analysis of multi-temporal Landsat images was achieved without downloading and performing time and memory-system-intensive tasks.

The proposed rainfall and multi-temporal flood analysis suggested a strong connection between flooded areas and the ruling climatic conditions of the QGRW, with increases in precipitation during the summer, and increases in flooded areas attributed to the decrease in evapotranspiration that arises during the winter. In the case of frequency analysis, the dominance of *Very Low* frequencies of flooding (AWPF < 20%) observed in both OFS and FV areas, highlighted the importance of flash flood events in the knowledge of areas potentially prone to flooding expected in plain watersheds.

The differentiation of OFS and FV from non-flooded areas was achieved by the combination of MNDWI and NDVI, with the NDVI as a powerful tool to evaluate the vegetation response to flooding. Here, the application of the Otsu method to compute the dynamic segmentation of the normalized difference histograms was a key step to define the dynamic threshold values according to the fractional components of water, soil, and vegetation, instead of using constant values.

Overall, this study provided valuable information for flood management and mitigation efforts in Argentina's agriculturally dominated river watersheds. Implementing these mapping techniques on a broader scale can contribute to more effective

preparedness, response, and recovery strategies for flood-prone regions in Argentina and beyond.

#### DATA AVAILABILITY

The codes developed in the current study are available in the Google Earth Engine platform: <https://code.earthengine.google.com/b5645a358ff74f7c0286624f4451e6d3> for multi-temporal flood analysis, and for annual flood frequency mapping: <https://code.earthengine.google.com/79eff9484ce89ef2bc402677d18284c1>.

#### ACKNOWLEDGMENTS

This work was financially supported by the National Agency for Scientific and Technological Promotion (PICT 1616/14), the National University of Mar del Plata (R354220), and the International Atomic Energy Agency's Coordinated Research Project (F30059) entitled "Assessment of Groundwater Resources at Local/National Scales". The authors give posthumous thanks to Ms. Joanie López Pueyredón, who performed a very important role in monitoring and logistical support.

#### REFERENCES

- Antolini, F., Tate, E., Dalzell, B., Young, N., Johnson, K. & Hawthorne, P. L. (2020). Flood risk reduction from agricultural best management practices. *JAWRA Journal of the American Water Resources Association*, 56(1), 161-179. <https://doi.org/10.1111/1752-1688.12812>
- Aragón, R., Jobbágy, E. & Viglizzo, E. (2011). Surface and groundwater dynamics in the sedimentary plains of the Western Pampas (Argentina). *Ecohydrology* 4, 433-447. <https://doi.org/10.1002/eco.149>
- Azedou, A., Khatibi, A. & Lahssini, S. (2022). Characterizing fluvial geomorphological change using Google Earth Engine (GEE) to support sustainable flood management in the rural municipality of El Faid. *Arabian Journal of Geosciences*, 15, 413. <https://doi.org/10.1007/s12517-022-09674-3>
- Alderman, K., Turner, L. & Tong, S. (2012). Floods and human health: A systematic review. *Environment International*, 47, 37-47. <https://doi.org/10.1016/j.envint.2012.06.003>
- Borro, M., Morandeira, N., Salvia, M., Minotti, P., Perna, P. & Kandus, P. (2014). Mapping shallow lakes in a large South American floodplain: A frequency approach on multitemporal Landsat TM/ETM data. *Journal of Hydrology*, 512, 39-52. <https://doi.org/10.1016/j.jhydrol.2014.02.057>
- Campo de Ferreras, A. M. & Piccolo, M. C. (1999). Hidrogeomorfología de la cuenca del Río Quequén Grande, Argentina. *Papeles de Geografía*, 29. <https://revistas.um.es/geografia/article/view/45221>
- Campos, J., Sillero, N. & Brito, J. (2012). Normalized difference water indexes have dissimilar performances in detecting seasonal and permanent water in the Sahara - Sahel transition zone. *Journal of Hydrology* 464-465, 438-446. <https://doi.org/10.1016/j.jhydrol.2012.07.042>
- Dash, P. & Sar, J. (2020). Identification and validation of potential flood hazard area using GIS-based multi-criteria analysis and satellite data-derived water index. *Journal of Flood Risk Management*, 13(3), 1-14. <https://doi.org/10.1111/jfr3.12620>
- Detrembleur, S., Stilmant, F., Dewals, B., Erpicum, S., Archambeau, P. & Pirotton, M. (2015). Impacts of climate change on future flood damage on the river Meuse, with a distributed uncertainty analysis. *Natural Hazards*, 77, 1533-1549. <https://doi.org/10.1007/s11069-015-1661-6>
- DeVries, B., Huang, C., Armston, J., Huang, W., Jones, J. & Lang, M. (2020). Rapid and robust monitoring of flood events using Sentinel-1 and Landsat data on the Google Earth Engine. *Remote Sensing of Environment*, 240, 1-15. <https://doi.org/10.1016/j.rse.2020.111664>
- Domenikiotis, C., Loukas, A. & Dalezios, N. (2003). The use of NOAA/AVHRR satellite data for monitoring and assessment of forest fires and floods. *Natural Hazards and Earth System Sciences*, 3, 115-128. <https://doi.org/10.5194/nhess-3-115-2003>
- Du, S., Shi, P., Van Rompaey, A. & Wen, J. (2015). Quantifying the impact of impervious surface location on flood peak discharge in urban areas. *Natural Hazards*, 76, 1457-1471. <https://doi.org/10.1007/s11069-014-1463-2>
- European Commission - Directorate-General for Environment. (2021). Strengthening the synergies between agriculture and flood risk management in the European Union. *Publications Office of the European Union*, 31 pp. <https://doi.org/10.2779/128153>
- Fan, Y., Li, H. & Miguez-Macho, G. (2013). Global Patterns of Groundwater Table Depth. *Science*, 339, 940-943. <https://doi.org/10.1126/science.1229881>

- Feloni, E., Mousadis, I. & Baltas, E. (2019). Flood vulnerability assessment using a GIS-based multi-criteria approach – The case of Attica region. *Journal of Flood Risk Management*, *13*, 1-15. <https://doi.org/10.1111/jfr3.12563>
- Foga, S., Scaramuzza, P., Guo, S., Zhu, Z., Dilley Jr, R., Beckmann, T., Schmidt, G., Dwyer, J., Hughes, M. & Laue, B. (2017). Cloud detection algorithm comparison and validation for operational Landsat data products. *Remote Sensing of Environment*, *194*, 379-390. <https://doi.org/10.1016/j.rse.2017.03.026>
- Gorelick, N., Hancher, M., Dixon, M., Ilyushchenko, S., Thau, D. & Moore, R. (2017). Google Earth Engine: Planetary-scale geospatial analysis for everyone. *Remote Sensing of Environment*, *202*, 18–27. <https://doi.org/https://doi.org/10.1016/j.rse.2017.06.031>
- Haldane, J. (1948). Note on the Median of a Multivariate Distribution. *Biometrika*, *35*, 414-417. <https://doi.org/10.1093/biomet/35.3-4.414>
- Hawker, L., Neal, J., Tellman, B., Liang, J., Schumann, G., Doyle, C., Sullivan, J., Savage, J. & Tshimanga, R. (2020). Comparing earth observation and inundation models to map flood hazards. *Environmental Research Letters*, *15*, 1-13. <https://doi.org/10.1088/1748-9326/abc216>
- Houspanossian, J., Giménez, R., Whitworth-Hulse, J. I., Noretto, M. D., Tych, W., Atkinson, P. M., Rufino, M. C. & Jobbágy, E. G. (2023). Agricultural expansion raises groundwater and increases flooding in the South American plains. *Science*, *380*(6652), 1344-1348. <https://doi.org/10.1126/science.add5462>
- Houspanossian, J., Kuppel, S., Noretto, M., Di Bella, C., Oricchio, P., Barrucand, M., Rusticucci, M. & Jobbágy, E. (2018). Long-lasting floods buffer the thermal regime of the Pampas. *Theoretical and Applied Climatology*, *131*, 111-120. <https://doi.org/10.1007/s00704-016-1959-7>
- Jain, V. & Sinha, R. (2005). Response of active tectonics on the alluvial Baghmati River, Himalayan foreland basin, eastern India. *Geomorphology*, *70*, 339–356. <https://doi.org/10.1016/j.geomorph.2005.02.012>
- Ji, L., Zhang, L. & Wylie, B. (2009). Analysis of Dynamic Thresholds for the Normalized Difference Water Index. *Photogrammetric Engineering & Remote Sensing*, *75*(11), 1307–1317. <https://doi.org/10.14358/PERS.75.11.1307>
- Kumar, H., Karwariya, S. & Kumar, R. (2022). Google Earth Engine-Based Identification of Flood Extent and Flood-Affected Paddy Rice Fields Using Sentinel-2 MSI and Sentinel-1 SAR Data in Bihar State, India. *Journal of the Indian Society of Remote Sensing*, *50*, 791-803. <https://doi.org/10.1007/s12524-021-01487-3>
- Kuppel, S., Houspanossian, J., Noretto, M. & Jobbágy, E. (2015). What does it take to flood the Pampas?: Lessons from a decade of strong hydrological fluctuations. *Water Resources Research*, *51*, 2937–2950. <https://doi.org/10.1002/2015WR016966>
- Lal, P., Prakash, A. & Kumar, A. (2020). Google Earth Engine for concurrent flood monitoring in the lower basin of Indo-Gangetic-Brahmaputra plains. *Natural Hazards*, *104*, 1947-1952. <https://doi.org/10.1007/s11069-020-04233-z>
- Marini, M. F. & Piccolo, M. C. (2005). Hidrogeomorfología de la cuenca del río Quequén Salado, Argentina. *Investigaciones Geográficas*, *37*, 59-71. <https://doi.org/10.14198/INGEO2005.37.04>
- Martínez, D. E., Solomon, K., Quiroz Londoño, O., Dapeña, C., Massone, H., Benavente, M., Panarello, H. & Grondona, S. (2010). *Tiempo medio de residencia del flujo base en aguas superficiales de la llanura pampeana: aplicación de isótopos del agua, gases nobles y CFCs en el río Quequén Grande*. In: I Congreso Internacional de Hidrología de Llanuras Azul, Buenos Aires, Argentina, 420-427.
- Martínez, D. E. & Bocanegra, E. M. (2002). Hydrogeochemistry and cation-exchange processes in the coastal aquifer of Mar Del Plata, Argentina. *Hydrogeology Journal*, *10*, 393–408. <https://doi.org/10.1007/s10040-002-0195-7>
- McFeeters, S. (1996). The Use of Normalized Difference Water Index (NDWI) in the Delineation of Open Water Features. *International Journal of Remote Sensing*, *17*(7), 1425–1432. <https://doi.org/10.1080/01431169608948714>
- Mehmood, H., Conway, C. & Perera, D. (2021). Mapping of Flood Areas Using Landsat with Google Earth Engine Cloud Platform. *Atmosphere*, *12*(7), 1-16. <https://doi.org/10.3390/atmos12070866>
- Mohammadi, A., Costelloe, J. & Ryu, D. (2017). Application of time series of remotely sensed normalized difference water, vegetation and moisture indices in characterizing flood dynamics of large-scale arid zone floodplains. *Remote Sensing of Environment*, *190*, 70–82. <https://doi.org/10.1016/j.rse.2016.12.003>
- Mora, D., Walker, E. & Venturini, V. (2021). Flood monitoring in Santa Fe using the Google Earth Engine platform. In: *XIX Workshop on Information Processing and Control (RPIC)*, 1-6. <https://doi.org/10.1109/RPIC53795.2021.9648518>
- Otsu, N. (1979). A Threshold Selection Method from Gray-Level Histograms. *IEEE Transactions on Systems, Man, and Cybernetics*, *9*, 62–66.

- Pandey, A., Kaushik, K. & Parida, B. (2022). Google Earth Engine for Large-Scale Flood Mapping Using SAR Data and Impact Assessment on Agriculture and Population of Ganga-Brahmaputra Basin. *Sustainability*, 14(7), 4210, 1-22. <https://doi.org/10.3390/su14074210>
- Paruelo, J., Guerschman, J. & Verón, S. R. (2005). Expansión agrícola y cambios en el uso del suelo. *Ciencia Hoy*, 15(87), 14–23.
- Policelli, F., Slayback, D., Brakenridge, B., Nigro, J., Hubbard, A., Zaitchik, B., Carroll, M. & Jung, H. (2017). The NASA Global Flood Mapping System. *Remote Sensing of Hydrological Extremes*, 47–63. [https://doi.org/10.1007/978-3-319-43744-6\\_3](https://doi.org/10.1007/978-3-319-43744-6_3)
- Powell, S., Jakeman, A. J. & Croke, B. (2014). Can NDVI response indicate the effective flood extent in macrophyte dominated floodplain wetlands? *Ecological Indicators*, 45, 486–493. <https://doi.org/10.1016/j.ecolind.2014.05.009>
- Quiroz Londoño, O., Grondona, S., Massone, H., Farenga, M., Martínez, G. & Martínez, D. (2013). Modelo de anegamiento y estrategia de predicción–prevención del riesgo de inundación en áreas de llanura: el sudeste de la provincia de Buenos Aires como caso de estudio. *GeoFocus. International Review of Geographical Information Science and Technology*, 13\_1, 76–98. <https://www.geofocus.org/index.php/geofocus/article/view/262>
- Robinson, N., Allred, B., Jones, M., Moreno, A., Kimball, J., Naugle, D., Erickson, T. & Richardson, A. (2017). A Dynamic Landsat Derived Normalized Difference Vegetation Index (NDVI) Product for the Conterminous United States. *Remote Sensing*, 9(8), 863,1-14. <https://doi.org/10.3390/rs9080863>
- Rogers, A. S. & Kearney, M., (2004). Reducing signature variability in unmixed coastal marsh Thematic Mapper scenes using spectral indices. *International Journal of Remote Sensing*, 25(12), 2317–2335. <https://doi.org/10.1080/01431160310001618103>
- Roy, D., Kovalskyy, V., Zhang, H., Vermote, E., Yan, L., Kumar, S. & Egorov, A. (2016). Characterization of Landsat-7 to Landsat-8 reflective wavelength and normalized difference vegetation index continuity. *Remote Sensing of Environment*, 185, 57-70. <https://doi.org/10.1016/j.rse.2015.12.024>
- Rozenberg, J., Dborin, D. V., Giuliano, F. M., Jooste, C., Mikou, M., Rodriguez Chamussy, L., Schwerhoff, G., Turner, S. D., Vezza, E. & Walsh, B. J. (2021). *Argentina - Poverty and Macro Economic Impacts of Climate Shocks (English)*. Washington, D.C.: World Bank Group. <http://documents.worldbank.org/curated/en/590371624981025569/Argentina-Poverty-and-Macro-Economic-Impacts-of-Climate-Shocks>
- Sandoval, V. & Sarmiento, J. (2020). A neglected issue: informal settlements, urban development, and disaster risk reduction in Latin America and the Caribbean. *Disaster Prevention and Management*, 29, 731–745. <https://doi.org/10.1108/DPM-04-2020-0115>
- Scarpati, O. E. & Capriolo, A. D (2013). Droughts and floods in Buenos Aires province (Argentina) and their space and temporal distribution. *Investigaciones Geográficas*, 82, 38–51. <https://doi.org/10.14350/rig.31903>
- Sethre, P., Rundquist, B. & Todhunter, P. (2005). Remote Detection of Prairie Pothole Ponds in the Devils Lake Basin, North Dakota. *GIScience & Remote Sensing*, 42(4), 277–296. <https://doi.org/10.2747/1548-1603.42.4.277>
- Shrestha, R., Di, L., Yu, E., Kang, L., Shao, Y. & Bai, Y. (2017). Regression model to estimate flood impact on corn yield using MODIS NDVI and USDA cropland data layer. *Journal of Integrative Agriculture*, 16(2), 398–407. [https://doi.org/10.1016/S2095-3119\(16\)61502-2](https://doi.org/10.1016/S2095-3119(16)61502-2)
- Solana, M. X., Quiroz Londoño, O. M., Weinzettel, P. & Donna, F. (2021a). Contributions to the conceptual hydrogeological model of the Quequén Grande River Basin at its southwestern limit. *Boletín Geológico y Minero*, 132(1-2): 197-205. <https://doi.org/10.21701/bolgeomin.132.1-2.020>
- Solana, M. X., Quiroz Londoño, O. M., Romanelli, A., Donna, F., Martínez, D. & Weinzettel, P. (2021b). Connectivity of temperate shallow lakes to groundwater in the Pampean Plain, Argentina: A remote sensing and multi-tracer approach. *Groundwater for Sustainable Development*, 13, 1-10. <https://doi.org/10.1016/j.gsd.2021.100556>
- Tellman, B., Sullivan, J. A. & Doyle, C. S. (2021). Global Flood Observation with Multiple Satellites. In: *Global Drought and Flood* (eds H. Wu, D.P. Lettenmaier, Q. Tang and P.J. Ward), 99–121. <https://doi.org/10.1002/9781119427339.ch5>
- Teruggi, L., Martínez, G., Billi, P. & Preciso, E. (2005). Geomorphologic units and sediment transport in a very low relief basin: Rio Quequén Grande, Argentina. *IAHS Publication*, 299, 154–160.
- Tsyganskaya, V., Martinis, S., Marzahn, P. & Ludwig, R. (2018). SAR-based detection of flooded vegetation – a review of characteristics and approaches. *International Journal of Remote Sensing*, 39(8), 2255–2293. <https://doi.org/10.1080/01431161.2017.1420938>

- Tucker, C. J. (1979). Red and photographic infrared linear combinations for monitoring vegetation. *Remote Sensing of Environment*, 8(2), 127-150. [https://doi.org/10.1016/0034-4257\(79\)90013-0](https://doi.org/10.1016/0034-4257(79)90013-0)
- UN-OCHA (2020). Natural disasters in Latin American and the Caribbean, 2000–2019. *New York: United Nations Office for the Coordination of Humanitarian Affairs*. <https://www.unocha.org/publications/report/world/natural-disasters-latin-america-and-caribbean-2000-2019>
- United State Geological Survey. (s.f.). *Landsat Known Issues*. <https://www.usgs.gov/core-science-systems/nli/landsat/landsat-known-issues>
- Vanama, V. S. K., Mandal, D. & Rao, Y. S. (2020). GEE4FLOOD: Rapid mapping of flood areas using temporal Sentinel-1 SAR images with Google Earth Engine cloud platform. *Journal of Applied Remote Sensing*, 14(3), 1-23. <https://doi.org/10.1117/1.JRS.14.034505>
- Wannous, C. & Velasquez, G. (2017). United Nations Office for Disaster Risk Reduction (UNISDR)—UNISDR’s Contribution to Science and Technology for Disaster Risk Reduction and the Role of the International Consortium on Landslides (ICL). In: Sassa, K., Mikoš, M., Yin, Y. (eds) *Advancing Culture of Living with Landslides*, 109-115. [https://doi.org/10.1007/978-3-319-59469-9\\_6](https://doi.org/10.1007/978-3-319-59469-9_6)
- Warner, B. P., Schattman, R. E. & Hatch, C.E. (2017). Farming the floodplain: Ecological and agricultural tradeoffs and opportunities in river and stream governance in New England’s changing climate. *Case Studies in the Environment*, 1(1), 1-9. <https://doi.org/10.1525/cse.2017.sc.512407>
- World Bank (2021). *Argentina: Valuing Water -Brief for Policy Makers*. Water Security Diagnostic, 1-27. <https://documents1.worldbank.org/curated/en/945671624438916229/pdf/Argentina-Water-Security-Valuing-Water-Brief-for-Policy-Makers.pdf>
- Wulder, M. A. & Coops, N. C. (2014). Satellites: Make Earth observations open access. *Nature*, 513, 30–31. <https://doi.org/10.1038/513030a>
- Xu, H. (2006). Modification of Normalized Difference Water Index (NDWI) to Enhance Open Water Features in Remotely Sensed Imagery. *International Journal of Remote Sensing*, 27(14), 3025–3033. <https://doi.org/10.1080/01431160600589179>

**Type of publication: ARTICLE**

**Received on 08/15/2023, approved for publication on 11/20/2023 and published on 12/12/2023.**

## CITATION

Solana, M. X., Romanelli, A. and Quiroz Londoño, O. M. (2023). Multi-temporal flood mapping and farm flood prevention strategies in an agriculturally dominated watershed of Argentina. *Cuadernos del CURIHAM*, 29. e191. <https://doi.org/10.35305/curiham.v29i.e191>

## AUTORSHIP ROLES

### Author contribution statement

María Ximena Solana: Conceptualization, Methodology, Developing codes in the GEE, Writing Original Draft. Asunción Romanelli: Investigation, Conceptualization, Writing, Reviewing and Editing. Orlando Mauricio Quiroz Londoño: Original Idea, Project Administration, Funding Acquisition, Supervision, Reviewing and Editing.

### Disclosure statement

No potential conflict of interest was reported by the authors.

The authors approved the final version for publication and they are able to respond to all aspects of the manuscript.

## LICENSE

*This is an open access article under license: Creative Commons Attribution-NonCommercial-ShareAlike 4.0 International (CC BY-NC-SA 4.0 DEED) (<https://creativecommons.org/licenses/by-nc-sa/4.0/deed.es>)*

